Crystallographic and Electrochemical Hydrogen Storage Performances of $La_{0.75}Ce_{0.25}Ni_{3.80}Mn_{0.90}Cu_{0.30}(Fe_{0.43}B_{0.57})_x$ ($x = 0$-0.20) Alloys

Xianguang Shang[1,2], Shan Lu[3], Xianyun Peng[1], Yanping Fan[1,2,*], Baoqing Zhang[1,2], Zhi Zhang[1], Baozhong Liu[1,2,*]

[1] School of Materials Science & Engineering, Henan Polytechnic University, Jiaozuo 454000, China
[2] State Key Laboratory of Metastable Materials Science and Technology, Yanshan University, Qinhuangdao 066004, China
[3] Department of Mechanic and Electrical Engineering, Jiaozuo University, Jiaozuo 454000, China
[*]E-mail: bzliu@hpu.edu.cn; hpuforrest@hpu.edu.cn

Herein, a hyper-stoichiometry $Fe_{0.43}B_{0.57}$ addition was used to improve the electrochemical hydrogen storage characteristics of Co-free high-Mn alloy. Microstructures and electrochemical performances of $La_{0.75}Ce_{0.25}Ni_{3.80}Mn_{0.90}Cu_{0.30}(Fe_{0.43}B_{0.57})_x$ ($x = 0$-0.20) alloys are investigated. X-ray diffraction and backscattered electron results indicate that the pristine alloy is $LaNi_5$ phase, while the alloys containing $Fe_{0.43}B_{0.57}$ consist of $LaNi_5$ matrix phase and $La_3Ni_{13}B_2$ secondary phase. The relative abundance of $La_3Ni_{13}B_2$ phase increases, and the *a*, *c* and *V* of $LaNi_5$ phase decrease with increasing *x* value. Maximum discharge capacity of the alloy electrodes monotonically decreases from 329.1 mAh/g ($x = 0$) to 314.7 mAh/g ($x = 0.20$). High-rate dischargeability of the alloy electrodes first increases with increasing *x* from 0 to 0.10, and then decreases until *x* increases to 0.20. Cycling capacity retention rate at the 100th cycle increases from 51.1% ($x = 0$) to 72.2% ($x = 0.20$) with increasing *x* value, which is ascribed to the improvement in pulverization resistance. It is demonstrated that the addition of $Fe_{0.43}B_{0.57}$ is an effective approach to improve the comprehensive electrochemical performances of Co-free high-Mn alloy electrodes.

1. INTRODUCTION

Nickel/metal hydride (Ni/MH) secondary batteries have been adopted in various portable electronic devices, and are serving in almost all commercial Ni/MH batteries AB_5-type alloys as

negative electrode materials due to their good overall electrode properties [1]. High cost of cobalt (Co) in AB_5 alloy motives the researchers to develop low Co or Co-free AB_5-type hydrogen storage alloys [2]. Many attempts have been made by substituting Co with foreign metals, such as, Mn, Fe, Cu, Si, etc [3-5], and thereafter the Co-free high-Mn alloys were developed and commercially produced due to high performance/cost ratio [6]. However, the electrochemical performances, especially high-rate dischargeability and cycling stability, of Co-free high-Mn alloys are not yet satisfying.

Non-stoichiometry is considered as a special doping and multicomponent alloying technique for intermetallic compounds, and can effectively improve the electrochemical hydrogen storage properties of AB_5-type alloys [7]. Deviating AB_5-type compound composition from a stoichiometry to hyper-stoichiometry contributed to high-rate dischargeability and cycling stability of hydrogen storage alloy [8, 9]. Therefore, adding hyper-stoichiometry element is always used to modify microstructure and hydrogen storage performances of AB_5 alloy [10-12].

Ye et al. [13] reported that the addition of boron modified the activation performance and significantly improved the high-rate capacity of $Mm_{3.55}Co_{0.75}Mn_{0.4}Al_{0.3}B_x$ alloy though the electrochemical capacity is lower than that of commercial $Mm_{3.55}Co_{0.75}Mn_{0.4}Al_{0.3}$ alloy. Zhang et al. [14] studied low Co AB_5-type $MmNi_{3.8}Co_{0.4}Mn_{0.6}Al_{0.2}B_x$ alloys and pointed out that the addition of B made the cycling stability improved, activation performance modified, high rate discharge capability and discharge voltage increased. Obviously, the addition of B element and increasing stoichiometric ratio is effective to enhance activation performance, high-rate dischargeability and cycling stability. However, the pure B is very expensive and unpractical to be used in the Co-less or Co-free alloy. Fortunately, the price of commercial $Fe_{0.43}B_{0.57}$ alloy is less than 5% price of pure B, and the melting point of $Fe_{0.43}B_{0.57}$ alloy is much lower than that of pure B. More importantly, Fe introduction in AB_5 alloy can remarkably improve cycling stability due to the improvement in the anti-pulverization of alloy electrode [15,16]. Therefore, it can be expected that the overall electrochemical characteristics could be improved by adding $Fe_{0.43}B_{0.57}$ in Co-free high-Mn AB_5-type alloys.

Here, on the basis of the merits of $Fe_{0.43}B_{0.57}$ and the belief that the Fe and B additions may result in some noticeable modification of electrochemical hydrogen storage performances, microstructures and electrochemical hydrogen storage characteristics of $La_{0.75}Ce_{0.25}Ni_{3.80}Mn_{0.90}Cu_{0.30}(Fe_{0.43}B_{0.57})_x$ (x = 0-0.20) alloys have been investigated.

2. EXPERIMENTAL PROCEDURES

$La_{0.75}Ce_{0.25}Ni_{3.80}Mn_{0.90}Cu_{0.30}(Fe_{0.43}B_{0.57})_x$ (x = 0-0.20) alloys were synthesized by induction melting of the metal elements (La, Ce, Ni, Mn, Cu: 99.9% in purity and commercial Fe-B alloy contained 57.0 at.% B and the other were Fe and trace impurities.) in argon atmosphere, and then were annealed. The ingots were annealed by at 1223 K for 10 h in argon atmosphere with the pressure of 0.08 MPa.

X-ray diffraction (XRD) measurement was carried out on X'pert PROMPD X-ray diffractometer with Cu Kα radiation in the range from 20° to 80° with 0.02 °/min, and the results were analyzed by means of Rietveld refinement (using the software MAUD).

   The alloy powders of measuring electrodes were obtained by grinding the inner part of alloy ingots in Ar atmosphere. All measuring electrodes for test were prepared by cold pressing a mixture of 0.15 g alloy powders of 200-400 mesh and 0.75 g nickel carbonyl powders into a pellet of 10 mm in diameter under 15 MPa. Electrochemical measurements were performed at 298 K in a standard tri-electrode system, consisting of a working electrode (metal hydride), a counter electrode (Ni(OH)$_2$/NiOOH), and a reference electrode (Hg/HgO) with 6 mol/L KOH solution as electrolyte. Each electrode was charged for 7 h at 60 mA/g and discharged to -0.6 V versus Hg/HgO at 60 mA/g at 298 K. After every charging/discharging, the rest time was 10 min. In evaluating the high-rate dischargeability, discharge capacity of the alloy electrodes at different discharge current density was measured. The high-rate dischargeability (HRD, %) was defined as HRD=C_d/C_{max} × 100%, where C_d was the discharge capacity at the discharge current density I_d (I_d = 60, 300, 600, 900 and 1200 mA/g, respectively), and C_{max} was the maximum discharge capacity at the discharge current density of 60 mA/g. The electrochemical impedance spectrums (EIS) were performed on a PARSTAT 2273 Advanced Potentiostat/Galvanostat station by scanning in the frequency range of 100 kHz to 10 mHz at 50% depth of discharge (DOD) at 298 K. The potential step measurements were tested on the same instrument at 100% charge state. A +500 mV potential was applied and the discharge time was 3600 s.

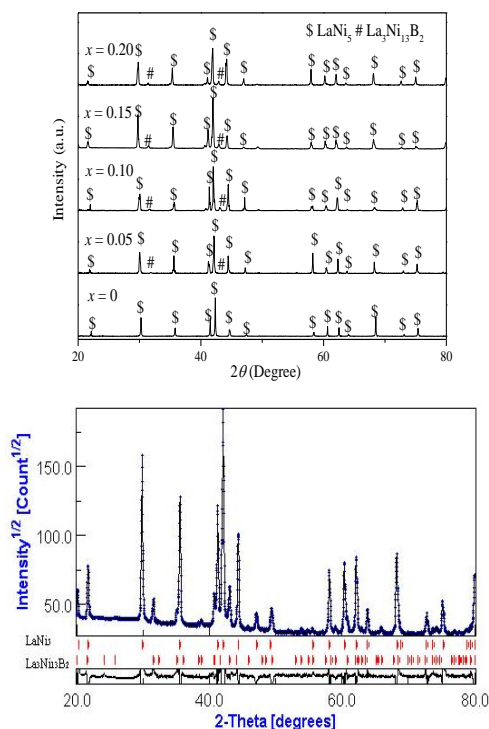## 3. RESULTS AND DISCUSSION

3.1 Crystal structure

Figure 1. XRD patterns of La$_{0.75}$Ce$_{0.25}$Ni$_{3.80}$Mn$_{0.90}$Cu$_{0.30}$(Fe$_{0.43}$B$_{0.57}$)$_x$ alloys (a) XRD patterns for x = 0-0.20 (b) Rietveld analysis pattern for x = 0.15

Table 1. The characteristics of phases in $La_{0.75}Ce_{0.25}Ni_{3.80}Mn_{0.90}Cu_{0.30}(Fe_{0.43}B_{0.57})_x$ alloys

Samples	Phases	Lattice parameter (Å)		Cell Volume (Å³)	Abundance (%)
$x = 0$	$LaNi_5$	$a = 5.072$	$c = 4.091$	91.14	100
$x = 0.05$	$LaNi_5$	$a = 5.072$	$c = 4.085$	90.99	96.43
	$La_3Ni_{13}B_2$	$a = 5.1055$	$c = 11.0407$		3.57
$x = 0.10$	$LaNi_5$	$a = 5.069$	$c = 4.078$	90.75	91.38
	$La_3Ni_{13}B_2$	$a = 5.1067$	$c = 11.0481$		8.62
$x = 0.15$	$LaNi_5$	$a = 5.059$	$c = 4.080$	90.44	90.25
	$La_3Ni_{13}B_2$	$a = 5.1075$	$c = 11.0576$		9.75
$x = 0.20$	$LaNi_5$	$a = 5.059$	$c = 4.075$	90.36	89.88
	$La_3Ni_{13}B_2$	$a = 5.1089$	$c = 11.0597$		10.12

Fig. 1a presents XRD patterns of $La_{0.75}Ce_{0.25}Ni_{3.80}Mn_{0.90}Cu_{0.30}(Fe_{0.43}B_{0.57})_x$ alloys. Fig. 1b shows the XRD pattern and Rietveld analysis pattern of $La_{0.75}Ce_{0.25}Ni_{3.80}Mn_{0.90}Cu_{0.30}(Fe_{0.43}B_{0.57})_{0.15}$ alloy. As can be seen from Fig. 1a, $La_{0.75}Ce_{0.25}Ni_{3.75}Mn_{0.90}Cu_{0.35}$ alloy is $LaNi_5$ phase with $CaCu_5$ type hexagonal structure. The alloys containing $Fe_{0.43}B_{0.57}$ are composed of $LaNi_5$ matrix phase and $La_3Ni_{13}B_2$ secondary phase. Lattice parameters, cell volume and phase relative abundance of the alloys are listed in Table 1. The relative abundance of $La_3Ni_{13}B_2$ phase increases, and the lattice parameter a, c and cell volume V of $LaNi_5$ phase decrease with increasing x value from 0 to 0.20.

3.2 Activation capability and maximum discharge capability

The number of cycles (N_a) needed to reach the maximum capacity and maximum discharge capacity (C_{max}) of $La_{0.75}Ce_{0.25}Ni_{3.80}Mn_{0.90}Cu_{0.30}(Fe_{0.43}B_{0.57})_x$ alloy electrodes are given in Table 2. It is noted that the N_a of the alloy electrodes increases from 2 ($x = 0$) to 4 ($x = 0.20$) with increasing x value, which indicates that the addition of $Fe_{0.43}B_{0.57}$ lowers down the activation process. The initial activation in the first few cycles is usually attributed to the particle size reduction and surface reconstruction [17]. It is confirmed that increasing stoichiometry contributes to the anti-pulverization of the alloy due to good compound homogeneity and low internal stain [18]. The stoichiometric ratio increases with increasing x value, and then improves the anti-pulverization, which is detriment to the activation. Moreover, Zhang et al. [19] pointed out that the phase interface or grain boundary was buffer areas for the release of distortion and stress of crystal lattice in the charging/discharging process, and then restricted the pulverization. According to the XRD results, the $La_3Ni_{13}B_2$ second phase increases with increasing x values, which causes the increment of phase interface and then enhances ant-pulverization. This is also unfavorable to activation process. In addition, Wu et al. [20] reported the oxidation film formed on the alloy surface increased the additive internal energy, which led to the poorer activation performance. Due to the low surface energy of Fe, the increase in Fe content makes the surface oxide layer become thick and causes the increase in internal energy, and then degrades activation property. The C_{max} of the alloy electrodes decreases monotonically from 329.1 mAh/g ($x = 0$) to 314.7 mAh/g ($x = 0.20$) with increasing x value, which should be ascribed to

following factors. Firstly, the hydrogen storage capacity of $La_3Ni_{13}B_2$ phase is 157 mAh/g [20], which is much lower discharge capacity than $LaNi_5$ matrix phase. The $La_3Ni_{13}B_2$ phase gradually increases with increasing x value, which is unfavorable for the discharge capacity. Secondly, Brateng et al. [22] pointed out that the larger the cell volume is, the discharge capacity is the higher. The maximum discharge capacity is closely correlated with the unit cell volume of compound [23]. The V of the $LaNi_5$ phase decreases with increasing x value, which is detrimental to the discharge capacity. Thirdly, the increase in Fe content leads to the surface oxide film thicker, which degrades the charge-transfer reaction on the alloy surface, as well as decreases the number of activity sites on the alloy surface and then makes the diffusion of hydrogen from the inner to the surface more difficultly.

Table 2. Electrochemical properties of $La_{0.75}Ce_{0.25}Ni_{3.80}Mn_{0.90}Cu_{0.30}(Fe_{0.43}B_{0.57})_x$ alloy electrodes

x	C_{max} (mAh/g)	N_a[b]	HRD_{1200}[a] (%)	S_{100} (%)
0	329.1	2	67.5	51.1
0.05	324.2	3	70.4	55.1
0.10	321.6	3	76.8	62.0
0.15	317.8	3	74.5	65.5
0.20	314.7	4	63.5	72.2

[a] The high-rate dischargeability at the discharge current density of 1200 mA/g.
[b] The number of cycles needed to activate the electrode.

3.4 High-rate dischargeability and electrochemical kinetics

Fig. 2 shows the relationship between the high-rate dischargeability (HRD) and the discharge current density of $La_{0.75}Ce_{0.25}Ni_{3.80}Mn_{0.90}Cu_{0.30}(Fe_{0.43}B_{0.57})_x$ alloy electrodes. The HRD of the alloy electrodes first increases with increasing x from 0 to 0.10, and then decreases when x increases to 0.20. The HRD at the discharge current density of 1200 mA/g (HRD_{1200}) is listed in Table 2. It can be seen that HRD_{1200} first increases from 67.5% ($x = 0$) to 76.8% ($x = 0.10$), and then decreases to 63.5% ($x = 0.20$).

It is well known that the HRD of the metal-hydride electrodes is dominated by the charge-transfer reaction at the electrode/electrolyte interface and the hydrogen diffusion rate within the bulky alloy electrode, which are reflected in the value of surface exchange current density (I_0), being a measure of the catalytic activity of an alloy, as well as in the hydrogen diffusion coefficient (D), which characterizes the mass transport properties of an alloy electrode [25].

The EIS of $La_{0.75}Ce_{0.25}Ni_{3.80}Mn_{0.90}Cu_{0.30}(Fe_{0.43}B_{0.57})_x$ alloy electrodes at 50% DOD are shown in Fig. 3. On the basis of the equivalent circuit [26], the charge-transfer resistance values (R_{ct}) are obtained and listed in Table 3. The R_{ct} values of the alloy electrodes first decreases from 91.2 mΩ g ($x = 0$) to 65.1 mΩ g ($x = 0.10$), and then increases to 106.7 mΩ g ($x = 0.20$) with increasing x value.

Furthermore, the I_0 can also describe the charge-transfer process. The I_0 value can be calculated according to the following formula [27].
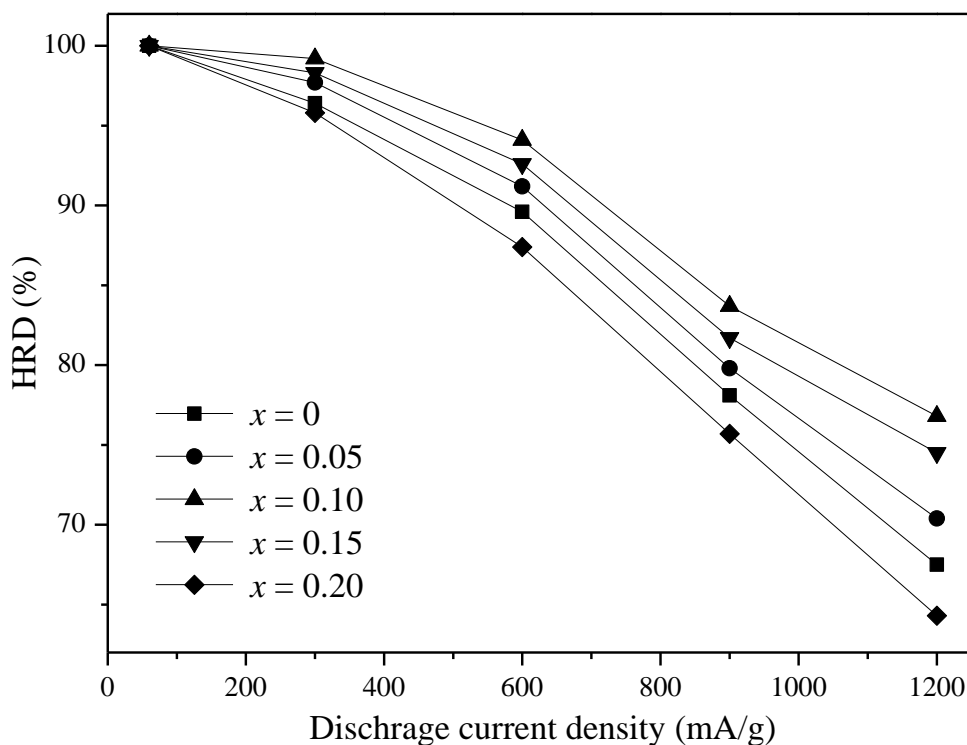
$$I_0 = \frac{RT}{FR_{ct}} \qquad (1)$$

Figure 2. HRD of $La_{0.75}Ce_{0.25}Ni_{3.80}Mn_{0.90}Cu_{0.30}(Fe_{0.43}B_{0.57})_x$ alloy electrodes

where R, T, F, R_{ct} are the gas constant, absolute temperature, Faraday constant and the polarization resistance, respectively. The I_0 values are calculated by Eq. (2) and listed in Table 3. It is clear that the I_0 first increases from 281.6 mA/g ($x = 0$) to 394.5 mA/g ($x = 0.10$), and then decreases to 240.7 mA/g ($x = 0.20$). It is reported that the formation of the $La_3Ni_{13}B_2$ secondary phase in AB_5 alloys improves the catalytic activity of the alloys [28]. As mentioned above, the secondary phase $La_3Ni_{13}B_2$ increases with increasing x value, which is of benefit to improve the electrocatalytic activity of the surface of alloy electrode and the charge-transfer reaction. Moreover, the addition of B contributes to the electrochemical activity [29], which is favorable to the charge-transfer reaction of the alloy electrodes. Unfortunately, the increase in Fe content on the alloy surface with increasing x value degrades the charge-transfer reaction because of the increase of oxide film on the alloy surface. Therefore, it is reasonable to assume that, when $x \leq 0.10$, the favorable effect is chiefly responsible for the increase of the exchange current density for alloy electrodes. However, when $x > 0.10$, the decrease of the exchange current density for alloy electrodes is mainly ascribed to the disadvantageous factors. Consequently, the threshold content of $Fe_{0.43}B_{0.57}$ is 0.10 in present system.
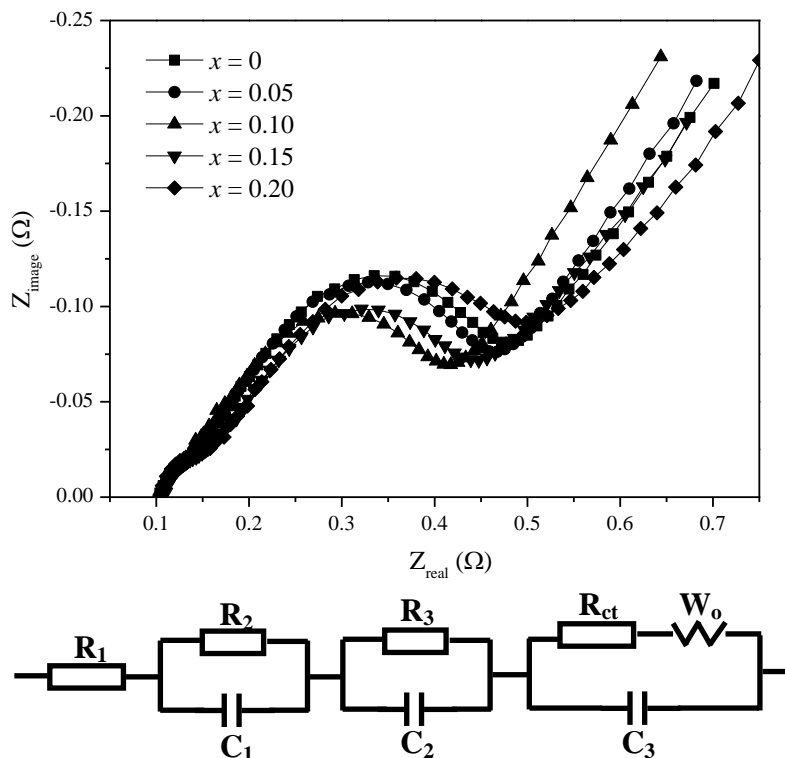
Figure 3. EIS of $La_{0.75}Ce_{0.25}Ni_{3.80}Mn_{0.90}Cu_{0.30}(Fe_{0.43}B_{0.57})_x$ alloy electrodes

Fig. 4 shows the semi-logarithmic plots of the anodic current vs. the time response of $La_{0.75}Ce_{0.25}Ni_{3.80}Mn_{0.90}Cu_{0.30}(Fe_{0.43}B_{0.57})_x$ alloy electrodes. It can be seen that the current-time responses can be divided into two time domains [30], in the first time region, the oxidation current of hydrogen rapidly declines due to the rapid consumption of hydrogen on the surface. However, in the followed second time region, the current declines more slowly and drops linearly with time. Zheng et al. [30] reported that in a large anodic potential-step test, after a long discharge time, the diffusion current varies with time according to the following equation:

$$\lg i = \lg(\frac{6FD}{da^2}(C_0 - C_s)) - \frac{\pi^2}{2.303}\frac{D}{a^2}t \qquad (2)$$

where i is anodic current density (A/g), D the hydrogen diffusion coefficient (cm^2/s), d the density of the alloy (g/cm^3), a the radius of the alloy particle, C_0 the initial hydrogen concentration in the bulk of the alloy (mol/cm^3), C_s the surface hydrogen concentration of the alloy (mol/cm^3) and t is the discharge time (s). Assuming that the alloy has a similar particle distribution with an average particle radius of 13 μm according to previous study [31], D was calculated and summarized in Table 3. The D of $La_{0.75}Ce_{0.25}Ni_{3.80}Mn_{0.90}Cu_{0.30}(Fe_{0.43}B_{0.57})_x$ alloy electrodes first increases from 6.53×10^{-11} ($x = 0$) to 8.60×10^{-11} cm^2/s ($x = 0.10$), and then decreases to 5.58×10^{-11} cm^2/s ($x = 0.20$). As mentioned above, the formation of the secondary phase increases the fraction of phase boundaries, which provides extra tunnels for the diffusion of hydrogen atoms. The increase of $La_3Ni_{13}B_2$ secondary phase causes the increase in the phase boundary, which can decrease the lattice distortion and strain energy formed in the process of hydrogen absorption. Moreover, it is well known that the A-side lanthanide atoms form the stable metal hydrides, while the B-side transitional atoms form the unstable metal hydrides.

The lower hydride stability facilitates the release of bonded hydrogen, which is favorable to the hydrogen diffusion of the alloys [32]. The addition of $Fe_{0.43}B_{0.57}$ results in the decrement of A-side atoms and the increment of B-side transitional atoms, which lowers the stability of the alloy hydride and then accelerates hydrogen diffusion. Conversely, Khaldi et al. [33] have reported that the oxidation of Fe on the alloy surface limited the hydrogen transfer from the surface to the bulk. As mentioned above, the increase of Fe content causes the increase of surface oxide film, which will degrade the hydrogen diffusion. Therefore, it is certain that the diffusion coefficient has a maximum value with increasing x value.

Iwakura et al. [34] have reported that linear dependence of the high-rate dischargeability on exchange current density and activation energy of hydrogen diffusion indicated that the charge transfer and hydrogen diffusion are responsible for discharge efficiency. Fig. 5 shows the HRD_{1200} as a function of exchange current density and hydrogen diffusion coefficient for $La_{0.75}Ce_{0.25}Ni_{3.80}Mn_{0.90}Cu_{0.30}(Fe_{0.43}B_{0.57})_x$ alloy electrodes. It is evident that the HRD_{1200} increases with the increase of I_0 and D, and shows a linear relationship with I_0 and D, respectively. This implies that both charge-transfer reaction at the electrode/electrolyte interface and the hydrogen diffusion of alloy electrodes should be responsible for the HRD at a discharge current density of 1200 mA/g.
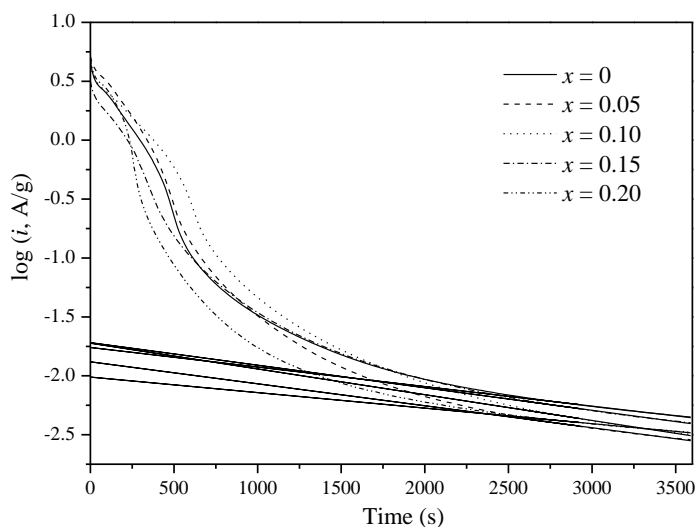

Figure 4. Semilogarithmic curves of anodic current vs. time of response of $La_{0.75}Ce_{0.25}Ni_{3.80}Mn_{0.90}Cu_{0.30}(Fe_{0.43}B_{0.57})_x$ alloy electrodes

Table 3. Electrochemical kinetic characteristics of $La_{0.75}Ce_{0.25}Ni_{3.80}Mn_{0.90}Cu_{0.30}(Fe_{0.43}B_{0.57})_x$ alloy electrodes

x	R_p (mΩ g)	I_0 (mA/g)	D ($\times 10^{-11}$ cm^2/s)
0	91.2	281.6	6.53
0.05	82.5	311.3	7.34
0.10	65.1	394.5	8.60
0.15	74.9	342.8	7.52
0.20	106.7	240.7	5.58

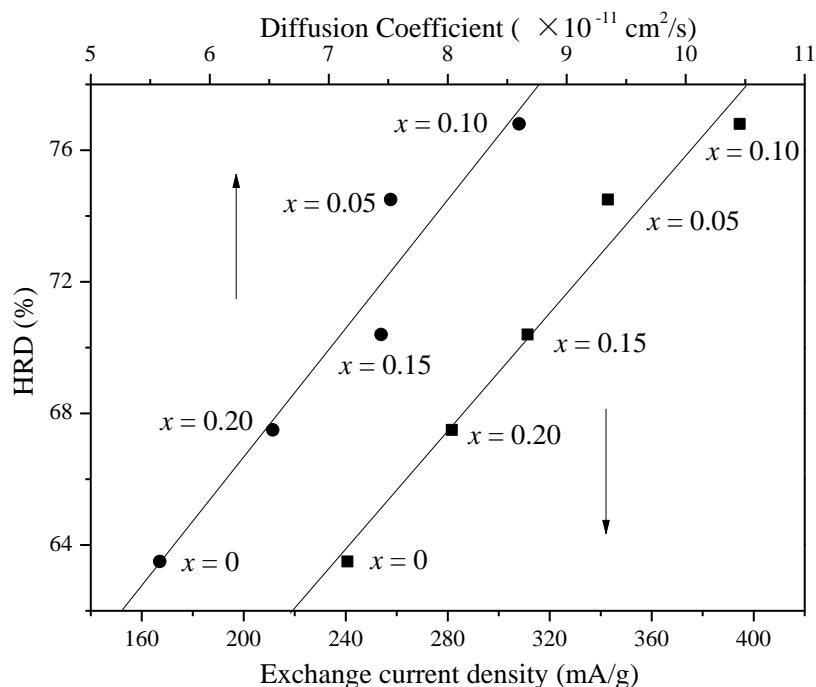**Figure 5.** HRD at 1200 mA/g as a function of exchange current density for $La_{0.75}Ce_{0.25}Ni_{3.80}Mn_{0.90}Cu_{0.30}(Fe_{0.43}B_{0.57})_x$ alloy electrodes

3.3 Cycling stability

Cycling stability is an extremely important factor for the service life of hydrogen storage alloys. The cycling capacity retention rate is expressed as $S_n(\%) = C_n/C_{max} \times 100$ (where C_n is the discharge capacity at the nth cycle). The cycling capacity retention rate of $La_{0.75}Ce_{0.25}Ni_{3.80}Mn_{0.90}Cu_{0.30}(Fe_{0.43}B_{0.57})_x$ alloy electrodes as a function of cycle number is shown in Fig. 6. Obviously $Fe_{0.43}B_{0.57}$ addition conduces to the cycling stability of alloy electrodes. The S_{100} of the alloy electrodes are listed in Table 2. It can be seen that S_{100} increases from 51.1% ($x = 0$) to 72.2% ($x = 0.20$). The fundamental reasons for the capacity decay of alloy electrode are attributed to the pulverization and corrosion of the alloy in the charging-discharging cycle [35, 36]. As mentioned above, the phase interface or grain boundary was buffer areas for the release of distortion and stress of crystal lattice in the charging/discharging process, and then restricted the pulverization [19]. The increment of $La_3Ni_{13}B_2$ second phase causes the increment of phase interface and then enhance ant-pulverization and the cycling stability. Moreover, it is well accepted that alloy having a smaller volume expansion on hydriding would lead to a lower degree of pulverization and thus exposes less surface area to the corrosive electrolyte, and hence corrodes less and has a better cycling stability [37]. Fe addition can strongly reduce the lattice expansion, and the decrease of lattice expansion suppresses the pulverization [38]. Increasing Fe content with increasing x value will restrain lattice expansion in the charging process and then enhance the pulverization resistance, which is favorable to the cycling stability. Unfortunately, it is well-known that Fe easily oxidized due to the lower surface energy and forms coarse oxide film. The increase in Fe content not only causes the deterioration of corrosion resistance and then increases the loss of the alloy, but also degrades the electrochemical kinetics on the

alloy surface, which is detrimental to the discharge capacity. Thus, it is reasonable to believe that the improvement in pulverization resistance of alloy electrode is one of critical reasons for the increment of cycling stability in present work.
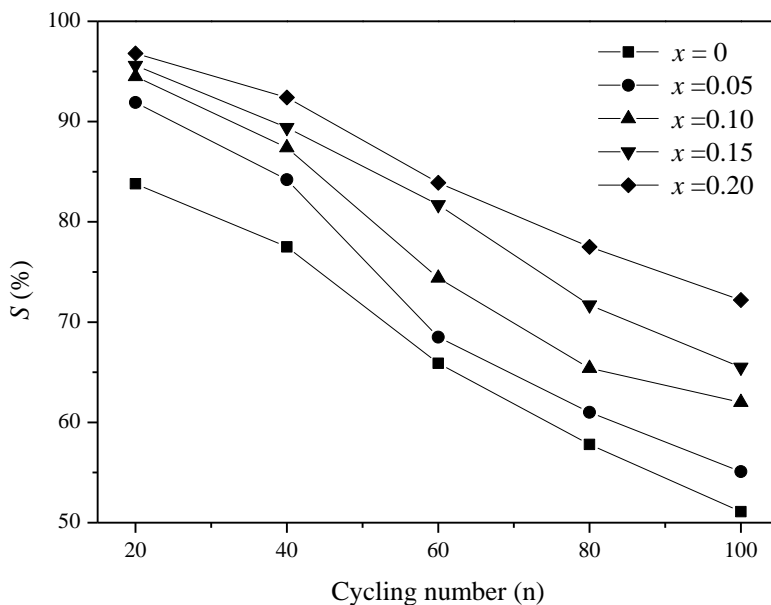

Figure 6. Cycling stability of $La_{0.75}Ce_{0.25}Ni_{3.80}Mn_{0.90}Cu_{0.30}(Fe_{0.43}B_{0.57})_x$ alloy electrodes

4. CONCLUSIONS

On the basis of microstructures and electrochemical characteristics of $La_{0.75}Ce_{0.25}Ni_{3.80}Mn_{0.90}Cu_{0.30}(Fe_{0.43}B_{0.57})_x$ hydrogen storage alloys, the following conclusions can be drawn:

● Bimodal microstructures of $LaNi_5$ matrix and $La_3Ni_{13}B_2$ secondary phase are observed in $La_{0.75}Ce_{0.25}Ni_{3.80}Mn_{0.90}Cu_{0.30}(Fe_{0.43}B_{0.57})_x$ alloys. Moreover, the relative abundance of $La_3Ni_{13}B_2$ increases with the increment of *x* value.

● Activation property and maximum discharge capacity of the alloy electrodes degrades with increasing $Fe_{0.43}B_{0.57}$ content.

● HRD_{1200} first increases from 67.5% (*x* = 0) to 76.8% (*x* = 0.10), and then decreases to 63.5% (*x* = 0.20), which is determined by the exchange current density and hydrogen diffusion coefficient.

● Adding $Fe_{0.43}B_{0.57}$ effectively conduces to the cycling stability of alloy electrodes, which is mostly affected by the improvement in the anti-pulverization.

References

1. S. Shi, C. Li and W. Tang, *J. Alloys Compd.*, 476 (2009) 874
2. X. Wei, S. Liu, H. Dong, P. Zhang, Y. Liu, J. Zhu and G. Yu, *Electrochim. Acta*, 52 (2007) 2423
3. Y.P. Zhao, Y.H. Zhang, G.Q. Wang, X.P. Dong, S.H. Guo and X.L. Wang, *J. Alloys Compd.*, 388 (2005) 284
4. B. Zhang, W.Y. Wu, X. Bian and G.F. Tu, *J. Alloys Compd.*, 538 (2012) 189
5. R. Tang, Y. Liu, C. Zhu, J. Zhu and G. Yu, *Intermetallics*, 14 (2006) 361
6. K. Komori, O. Yamamoto, Y. Toyoguchi, K. Suzuki, S. Yamaguchi, A. Tanaka and M. Ikoma, US5512385 (1996)
7. C.Y. Seo, S. J. Choi, J. Choi, C.N. Park and J.Y. Lee, *Int. J. Hydrogen Energy*, 28 (2003) 967
8. S.L. Li, P. Wang, W. Chen, G. Luo, D. Chen and K. Yang, *Int. J. Hydrogen Energy*, 28 (2003) 1101
9. K.Y. Shu, S.K. Zhang, Y.Q. Lei, G.L. Lu and Q.D. Wang, *Int. J. Hydrogen Energy*, 28 (2003) 1101
10. C.Y. Seo, S.J. Choi, J. Choi, C.N. Park and J.Y. Lee, *J. Alloys Compd.*, 351 (2003) 255
11. C. Iwakura, K. Ohkawa, H. Senoh and H. Inoue, *Electrochim. Acta*, 46 (2001) 4383
12. K. Young, T. Ouchi, B. Reichman, J. Koch, and M.A. Fetcenko, *J. Alloys Compd.*, 509 (2011) 3995
13. H. Ye, H. Zhang, W.Q. Wu and T.S. Huang, *J. Alloys Compd.*, 312 (2000) 68
14. Y.H. Zhang, M.Y. Chen, X.L. Wang, G.Q. Wang, X.P. Dong and Y. Qi, *Electrochim. Acta*, 49 (2004) 1161
15. S.K. Pandey, A. Srivastava and O.N.Srivastava, *Int. J. Hydrogen Energy*, 32 (2007) 2461
16. M.B. Moussa, M. Abdellaoui, H. Mathlouthi, J. Lamloumi and A.P. Guegan, *J. Alloys Compd.*, 458 (2008) 410
17. G.D. Adzic, J.R. Johnson, J.J. Reilly, J. McBreen, S. Mukejee, M.P. Sridar Kumar, W. Zhang and S. Srinivasan, *J. Electrochem. Soc.*, 142 (1995) 3429
18. H. Ye, H. Zhang, J.X. Cheng and T.S. Huang, *J. Alloys Compd.*, 308 (2000) 163
19. Y. Zhao, Y. Zhang, G. Wang, X. Dong, S. Guo and X. Wang, *J. Alloys Compd.*, 388 (2005) 284
20. M.S. Wu, H.R. Wu, Y.Y. Wang and C.C. Wan, *J. Alloys Compd.*, 302 (2000) 248
21. H.Z. Yan, F.Q. Kong, W. Xiong, B.Q. Li, J. Li and L. Wang, *Int. J. Hydrogen Energy*, 35 (2010) 5687
22. R. Brateng, S. Gulbrandsen-Dahl, L.O. Vaøen, J.K. Solberg and R. Tunold, *J. Alloys Compd.*, 396 (2005) 100
23. Y. Fukmoto, M. Miyamoto, H. Inoue, M. Matsuoka and C. Iwakura, *J. Alloys Compd.*, 231 (1995) 562
24. P. Li, X.L. Wang, Y.H. Zhang, R. Li, J.M. Wu and X.H. Qu, *J. Alloys Compd.*, 353 (2003) 278
25. X.B. Zhang, D.Z. Sun, W.Y. Yin, Y.J. Chai and M.S. Zhao, *Chem. Phys. Phys. Chem.*, 6 (2005) 520
26. N. Kuriyama, T. Sakai, H. Miyamura, I. Uehara and H. Ishikawa, *J. Alloys Compd.*, 202 (1993) 183
27. P. Notten and P. Hokkeling, *J. Electrochem. Soc.*, 138 (1991) 1877
28. B.Z. Liu, M.J. Hu, L.Q. Ji, Y.P. Fan, Y.G. Wang, Z. Zhang and A.M. Li, *J. Alloys Compd.*, 516 (2012) 53

29. S.Q. Yang, S.M. Han, Y. Li, S.X. Yang and L. Hu, *Mater. Sci. Eng. B*, 176 (2010) 231
30. G. Zheng, B.N. Popov and R.E. White, *J. Electrochem. Soc.*, 142 (1995) 2695
31. B.Z. Liu, G.X. Fan, Y.C. Wang, G.F. Mi, Y.M. Wu and L.M. Wang, *Int. J. Hydrogen Energy*, 33 (2008) 5801
32. H. Ye, Y.X. Huang, J.X. Chen and H. Zhang, *J. Power Sources*, 103 (2002) 293
33. C. Khaldi, H. Mathlouthi, J. Lamloumi and A. Percheron-Guegan, *J. Alloys Compd.*, 360 (2003) 266
34. C. Iwakura, M. Miyamoto, H. Inoue, M. Matsuoka and Y. Fukumoto, *J. Alloys Compd.*, 259 (1997) 129
35. T. Sakai, H. Yoshinaga, H. Miyamura, N. Kuriyama and H. Ishikawa, *J. Alloys Compd.*, 180 (1992) 37
36. D. Chartouni, F. Meli, A. Zuttel, K. Gross and L. Schlapbach, *J. Alloys Compd.*, 241 (1996) 160
37. J.J. Reilly, G.D. Adzic, J.R. Johnson, T. Vogt, S. Mukerjee and J. McBreen, *J. Alloys Compd.*, 293–295 (1999) 569
38. S. Vivet, J.M. Joubert, B. Knosp and A. Percheron-Guégan, *J. Alloys Compd.*, 356–357 (2003) 779